In Review Submitted to WRR.

Development and Evaluation of a Mathematical Model For the Transport and Oxidation-Reduction of CoEDTA

James E. Saiers
School of Environmental Studies
Yale University
New Haven, CT 06511
james.saiers@yale.edu

Hillol Guha
Department of Geology
Florida International University
Miami, FL 33 199

Phil Jardine and **Scott Brooks**
Environmental Sciences Division
Oak Ridge National Laboratory
Oak Ridge, TN 3783 1

19 November 1999

Abstract

Oxidation-reduction reactions, catalyzed by iron and manganese oxides, influence the subsurface mobility of a variety of toxic metals. In the work reported here, we develop a new model for the transport of the redox-sensitive CoEDTA complex, and we test the model against published data on the movement of CoEDTA through columns packed with β-MnO_2-coated sand. The model solves equations for the advective-dispersive transport of three aqueous species: Co(II)EDTA, Co(III)EDTA, and dissolved oxygen. These transport equations are linked with nonlinear kinetics expressions that describe (1) oxidation of Co(II)EDTA to Co(III)EDTA by β-MnO_2, (2) inhibition of Co(II)EDTA oxidation due to precipitation of a Mn(III)-oxide, an insoluble reaction product that occludes the β-MnO_2 surface, and 3) regeneration of the redox-reactive β-MnO_2 surface through oxidation of the Mn(III) precipitate by porewater oxygen. Comparison of experimental and calculated results demonstrates that the model closely describes the response of the coupled hydrological and geochemical processes to changes in flow rate, influent concentrations of Co(II)EDTA, and β-MnO_2 surface coverages.

Introduction

Coupled processes, including advection, dispersion, and adsorption, govern the migration of dissolved contaminants in subsurface environments. In addition to these processes, oxidation-reduction reactions influence the fate and transport of a broad class of chemicals found in soil water and in groundwater. Cobalt is a redox-sensitive metal characterized by widespread occurrence in groundwater and high toxicity to humans and animals. Cobalt detected in groundwaters beneath several defense sites is complexed by EDTA, an organic chelating agent used in decontamination operations and disposed with cobalt in unlined trenches and pits [Means et al. 1978; Killey et al., 1984]. The transport characteristics of CoEDTA depend heavily on the oxidation state of the complex. Iron and manganese oxides, which exist ubiquitously in geologic environments as coatings on mineral grains, catalyze the transformation of Co(II)EDTA to Co(III)EDTA [Jardine et al., 1993; Xue and Traina, 1996]. Both Co(II)EDTA and Co(III)EDTA are anionic complexes, with the reduced species exhibiting a greater affinity to sorb to geologic solids than the oxidized species [Zachara et al., 1995a]. Relative to Co(III)EDTA, Co(II)EDTA is a far less stable complex and can be disassociated by Fe and Al oxides in soils and sediments [Girvin et al., 1993; Szecsody et al., 1994]. Once disassociated, Co mobility diminishes appreciably because free Co^{2+} binds tightly to geologic solids [Bums, 1976; Murray and Dillard, 1979].

Co(II)EDTA oxidation by iron and manganese oxides has been investigated in batch experiments [Jardine and Taylor, 1995a; Zachara et al. 1995b] and, to a lesser extent, in miscible-displacement experiments [Brooks et al., 1996; Szecsody et al., 1998a; Szescody et al., 1998b]. Jardine and Taylor [1995b] reported that the rates of Co(II)EDTA oxidation in columns of pyrolusite (β-MnO_2)-coated sand declined appreciably after a brief period of extremely rapid transformation; however, flushing the columns with oxygenated, CoEDTA-free water restored the original oxidative potential of the sand packs. The authors hypothesized that three processes

combined to produce this complex behavior: β-MnO_2-catalyzed oxidation of Co(II)EDTA to Co(III)EDTA, (2) formation of an insoluble Mn(III) precipitate that covered the reactive β-MnO_2 surface and impeded Co(II)EDTA oxidation, and (3) slow regeneration of β-MnO_2 through oxidation of the Mn(III) precipitate by dissolved oxygen. Fendorf et al. [1999] used XANES spectroscopy in coordination with a flow cell to identify the solid-phase reaction products of Co(II)EDTA. In accordance with the hypothesis of Jardine and Taylor [1995b], Fendorf et al. [1999] found that a thin layer of α-Mn_2O_3, a Mn(III) phase, formed on β-MnO_2 during Co(II)EDTA oxidation, and that the formation of this precipitate was coincident with the loss in the oxidative capacity of β-MnO_2 towards Co(II)EDTA.

The results of the laboratory experiments demonstrate that interactions between various geochemical processes produce complex effects on the movement of CoEDTA. A useful theory for the reactive transport of CoEDTA, as well as for the transport of other redox-sensitive contaminants, relies on the ability to quantify the kinetics of these interacting geochemical processes under conditions of advective-dispersive porewater flow. Mathematical models that quantify coupled advective-dispersive transport and oxidation-reduction are available [e.g., Liu and Narasimhan, 1989; Friedly et al., 1995; Yeh and Salvage, 1995], but, with few exceptions, these models have not been evaluated against experimental data [Szecsody et al., 1998a]. As a result, the identity of the complement of reactions that control the dynamics of oxidation-reduction remains uncertain, and thus, the appropriate forms of the mathematical equations that describe these reactions cannot be positively defined.

In this study, we begin to fill these gaps in existing knowledge. We present a new model for the transport and fate of redox-sensitive species, and we test this model against data reported by Jardine and Taylor [1995b] on the movement of CoEDTA through columns of β-MnO_2-coated

sand. The mathematical model solves equations for advection and dispersion of multiple aqueous species together with equations for rate-limited oxidation-reduction reactions. We find that, if the kinetics equations are formulated to account for the dependence of Co(II)EDTA oxidation rates on the build up of an insoluble Mn(III) precipitate and on regeneration of β-MnO_2 by reoxidation of this surface-bound precipitate, model calculations closely match observations from experiments conducted over a range of conditions. This work illuminates the network of physical and chemical processes that contribute to CoEDTA transport and transformation in manganese-containing sediments and is the first to rigorously quantify these processes.

Description of Column Experiments on CoEDTA Transport

We test the mathematical model against data from six experiments on the transport of CoEDTA through water-saturated columns packed with pyrolusite (β-MnO_2)-coated quartz sand. Jardine and Taylor [1995b] provide a full description of the experimental methods; we summarize those methods here.

Two different sands, distinguished on the basis of β-MnO_2 surface coverage, were used in the column experiments. The columns were packed with fresh media for each of the three experiments with 0.4% (by weight) β-MnO_2-coated sand, and the transport of CoEDTA was measured in response to changes in influent Co(II)EDTA concentration and porewater velocity (Table 1). Three experiments, conducted at the same porewater velocity and same influent concentration of Co(II)EDTA, were run with the same column of 0.04% β-MnO_2-coated sand. In between each experiment with the 0.04% coated sand, the column was flushed with oxygen&d, CoEDTA-free water (Table 1). The oxic-water flushes were performed to determine if the oxidative capacity of the sand pack could be restored by oxidation of α-Mn_2O_3 to β-MnO_2.

The pyrolusite-coated sand used in the experiments was prepared by adding diluted $Mn(NO_3)_2$ to clean quartz sand, drying the sand at 433 K for 3 days, and washing the coated sand with 0.01 M $CaCl_2$ until the loss of pyrolusite into solution was negligible. The coated sand was wet packed to a height of 4.5 cm in vertically oriented, glass chromatography columns (1 cm i.d.). The pore volume of the sand packs measured 1.7 cm^3, corresponding to a porosity of 0.48 cm^3/cm^3. High-performance liquid chromatography pumps, positioned at the column inlet, controlled the upward flow of water and solutes through the sand beds.

During each experiment, Co(II)EDTA was applied to the bottom of the column as a step input, while samples of effluent were collected from the top of the column and analyzed for concentrations of Co(II)EDTA and Co(III)EDTA by ion chromatography. The influent solutions of Co(II)EDTA, which were kept in equilibrium with the atmosphere and had a dissolved O_2 concentration of 0.26 mM, were prepared in a background solution of 10 mM $CaCl_2$ by the stoichiometric addition of Ca_2EDTA to $CoCl_2 \cdot H_2O$. Co(II)EDTA was stable against oxidation by dissolved O_2, owing to the exceedingly slow rates of this kinetic reaction.

Overview of Experimental Results

CoEDTA Transport Through 0.4% Pyrolusite (β-MnO_2)-Coated Sand

Application of 0.2 mM Co(II)EDTA to a column packed with 0.4% coated sand produces rapid breakthrough of Co(III)EDTA (Figure 1). The high initial concentrations of Co(III)EDTA reflect rapid rates of β-MnO_2-catalyzed oxidation of Co(II)EDTA. With continued injection of Co(II)EDTA, a decline in effluent Co(III)EDTA concentrations signal a proportionate decline in Co(II)EDTA oxidation rates. According to Fendorf et al. [1999], this decrease in oxidation rates results from passivation of the β-MnO_2 surface by accumulation of α-Mn_2O_3, a solid-phase reaction product of Co(II)EDTA oxidation. Eventually, Co(III)EDTA concentrations stabilize at levels well above zero suggesting that, while diminished, the oxidative capacity of the column is not

completely exhausted over the duration of the Co(II)EDTA injection. Jardine and Taylor [1995b] speculate that reoxidation of α-Mn_2O_3 by porewater oxygen partially replenishes, solid-phase β-MnO_2 and effectively sustains low levels of Co(II)EDTA oxidation.

Concentrations of unreacted Co(II)EDTA increase coincidently with the decline in Co(III)EDTA concentrations, and as a result, the breakthrough curve for total CoEDTA (= Co(II)EDTA + Co(III)EDTA) nearly matches the breakthrough curve for bromide, a conservative tracer (Figure 1). The small deviation between the breakthrough curves of total CoEDTA and bromide indicates that sorptive interactions with the β-MnO_2-coated sand affect the movement of CoEDTA. In experiments in which Co(III)EDTA is used in place of Co(II)EDTA in the influent solution, Co(III)EDTA travels conservatively with a breakthrough that is identical that of bromide [Jardine and Taylor, 1995b]; thus, Co(II)EDTA represents the weakly sorbing species in the experiments reported here.

The transport of the organo-metallic complex is sensitive to variation in the influent concentration of Co(II)EDTA. A four-fold increase in influent concentration (from 0.2 mM to 0.8 mM) depletes the oxidative potential of the column more quickly and produces lower steady-state concentrations of Co(III)EDTA (Figures 2a, and 2b). CoEDTA breakthrough also responds to changes in porewater velocity (Figures 2a and 2c). With a four-fold increase in flow rate, the mass of Co(III)EDTA produced from the oxidation reaction and then eluted from the columns decreases by 15%. The dependence of Co(II)EDTA oxidation on porewater velocity demonstrates that the reaction is rate limited, or, in other words, the time scales for CoEDTA transport and for CoEDTA oxidation-reduction are comparable.

CoEDTA Transport Through 0.04% Pyrolusite (β-MnO_2)-Coated Sand

Results of three experiments conducted on the same column of 0.04% β-MnO_2-coated sand show that flushing the columns with oxygenated, CoEDTA-free porewater regenerates the oxidative potential of the sand bed (Figures 3a, 3b, and 3c). Co(II)EDTA is introduced to a freshly packed column of β-MnO_2 for a period of 44 pore volumes in the first experiment. After a brief period of rapid oxidation of Co(II)EDTA to Co(III)EDTA, the oxidative potential of the column diminishes until Co(III)EDTA concentrations in the column effluent stabilize at a relatively low level of C/C_0 = 0.2 (Figure 3a). Following this Co(II)EDTA injection, the columns are flushed for 12 pore volumes with a fully oxygenated $CaCl_2$ solution. This CoEDTA-free solution is applied at a rate of 10 cm^3/min, corresponding to a porewater velocity of 28 cm/h. Application of the 0.2 mM Co(II)EDTA solution is repeated after the 12-pore volume flush. Much of the original oxidative capacity of the sand bed is restored as concentrations of Co(III)EDTA increase from a level of C/C_0 = 0.2 at the end of the first experiment (Figure 3a) to a peak of C/C_0 = 0.75 near the beginning of the second experiment (Figure 3b). Nevertheless, as observed previously, Co(II)EDTA oxidation rates decline rapidly with time, eventually approaching a nonzero steady-state level (Figure 3b). After the second Co(II)EDTA injection, the column is flushed again with oxygenated $CaCl_2$ solution, this time for 23 pore volumes, and then Co(II)EDTA is introduced to the column for a final time. The increased flushing time results in greater restoration of system oxidative potential: Co(III)EDTA concentrations peak at C/C_0 = 0.9 after-the 23-pore volume flush, compared to C/C_0 = 0.75 after the initial 12-pore volume flush (Figures 3b and 3c).

Model Description

Transport of Aqueous Species

The numerical model accounts for the advective-dispersive transport of three aqueous species: Co(II)EDTA, Co(III)EDTA, and dissolved oxygen. We do not consider unchelated Co

species because these species were not detected in the column effluent during any of the column experiments and because results of speciation calculations made with GEOCHEM [Sposito and Mattigod, 1980; Parker et al., 1987] show that greater than 98% of Co(II) and Co(III) in the 10 mM $CaCl_2$ solutions is complexed by EDTA.

'We assume that the transport of both CoEDTA species is unaffected by adsorption. This assumption is strictly valid for Co(III)EDTA, which exhibits no affinity to bind to the β-MnO_2-coated sand and travels conservatively through the columns [Jardine and Taylor, 1995b]. The transport of Co(II)EDTA, however, is influenced by sorptive mass transfer, which retards the transport of Co(II)EDTA and serves as the initial step in the surface-catalyzed oxidation of Co(II)EDTA to Co(III)EDTA. Nevertheless, Co(II)EDTA retardation in the experiments is small, so model-data agreement is not jeopardized by excluding the effects of adsorption.

Oxidation-Reduction Reactions

Equations for nonlinear, kinetic oxidation-reduction reactions are coupled with the transport equations. We assume that β-MnO_2 is the sole oxidant for Co(II)EDTA and that the redox reaction generates Co(III)EDTA and α-Mn_2O_3, a Mn(III)-oxide solid. We derive the model equations for Co(II)EDTA oxidation from the chemical reaction proposed by Jardine and Taylor [1995b]:

$$\text{Co(II)EDTA} + MnO_2 + 0.5H_2O \rightarrow \text{Co(III)EDTA} + 0.5Mn_2O_3 + OH^- \qquad (1)$$

An alternate reaction scenario can be written with Mn^{2+}, instead of Mn_2O_3, as the product of β-MnO_2 reduction; however, we can dismiss this reaction scenario on the basis of two observations: (1) Mn^{2+} was not detected in effluent collected during the column experiments [Jardine and Taylor, 1995b] and (3) XANES analysis of β-MnO_2-coated sand reacted with Co(II)EDTA revealed the presence of surface-associated α-Mn_2O_3, but no surface-bound Mn^{2+} [Fendorf et al., 1999]. These observations also serve as evidence against the importance of α-Mn_2O_3 as a secondary oxidant of

Co(II)EDTA because significant oxidation of Co(II)EDTA by α-Mn_2O_3 would produce measurable quantities of Mn^{2+}.

We hypothesize that β-MnO_2, depleted in the oxidation-reduction reaction with Co(II)EDTA, can be regenerated in the presence of well-oxygenated porewater. The model equations for this process are based on the reaction

$$Mn_2O_3 + 0.5O_2 \rightarrow 2MnO_2 \qquad (2)$$

Once regenerated, solid-phase MnO_2 is again available to participate in oxidation-reduction reactions with Co(II)EDTA. Mn_2O_3 reoxidation to MnO_2 appears to be responsible for the longer term Co(II)EDTA oxidation (t > 6 pore volumes) observed in the column experiments.

Model Equations

The one-dimensional form of the advection-dispersion equation quantifies the spatial and temporal changes in the concentrations of the oxidized and reduced species of CoEDTA within the laboratory columns:

$$\frac{\partial[Co(II)]}{\partial t} = D\frac{\partial^2[Co(II)]}{\partial x^2} - v\frac{\partial[Co(II)]}{\partial x} + Q1_{Co(II)} \qquad (3)$$

$$\frac{\partial[Co(III)]}{\partial t} = D\frac{\partial^2[Co(III)]}{\partial x^2} - v\frac{\partial[Co(III)]}{\partial x} + Q1_{Co(III)} \qquad (4)$$

where [Co(II)] and [Co(III)] are the aqueous-phase concentrations of Co(II)EDTA and Co(III)EDTA, respectively, t is time, x is the coordinate parallel to flow, D is the hydrodynamic dispersion coefficient, and v is the average linear velocity. $Q1_{Co(II)}$ and $Q1_{Co(III)}$ are source/sink terms that describe the rates of species concentration change resulting from the oxidation-reduction reaction given by (1). The source/sink terms, which are defined below, are positive if the species'is generated in the reaction and negative if the species is consumed in the reaction.

An equation identical in form to equations (3) and (4) describes the movement of dissolved oxygen through the sand columns:

$$\frac{\partial[O_2]}{\partial t} = D\frac{\partial^2[O_2]}{\partial x^2} - v\frac{\partial[O_2]}{\partial x} + Q2_{O_2} \qquad (5)$$

where $[O_2]$ is the aqueous-phase oxygen concentration and $Q2_{O_2}$ quantifies temporal changes in oxygen concentration resulting from the oxidation-reduction reaction expressed by (2).

The solid-phase concentrations of β-MnO_2 and α-Mn_2O_3 are not affected directly by advective-dispersive transport processes, but vary only in response to redox reactions. The total change in β-MnO_2 concentrations is equal to the sum of $Q1_{MnO_2}$, the change in β-MnO_2 concentrations that arises from Co(II)EDTA oxidation, and $Q2_{MnO_2}$, the change in β-MnO_2 concentrations that arises from reoxidation of α-Mn_2O_3 by dissolved oxygen:

$$\frac{\rho}{\Theta}\frac{\partial[MnO_2]}{\partial t} = Q1_{MnO_2} + Q2_{MnO_2} \qquad (6)$$

where $[MnO_2]$ is the solid-phase concentration of β-MnO_2, ρ is the bulk density, and Θ is the porosity. Variations in solid-phase α-Mn_2O_3 occur concomitantly and are inversely proportional to changes in β-MnO_2 concentrations. As such, the mass balance equation for α-Mn_2O_3 is written as

$$\frac{\rho}{\Theta}\frac{\partial[Mn_2O_3]}{\partial t} = Q1_{Mn_2O_3} + Q2_{Mn_2O_3} \qquad (7)$$

where $[Mn_2O_3]$ is the solid-phase concentration of α-Mn_2O_3, $Q1_{Mn_2O_3}$ is the rate that α-Mn_2O_3 is generated from the reduction of β-MnO_2 by Co(II)EDTA and $Q2_{Mn_2O_3}$ is the rate that α-Mn_2O_3 is consumed through its oxidation by O_2.

Equations (3) – (7) represent the most general form of the mass balance equations for CoEDTA fate and transport. Solution of these equations requires specification of the rate laws that define the source-sink terms. We derive the mathematical relationship between $Q1_{Co(II)EDTA}$, $Q1_{Co(III)EDTA}$, $Q1_{MnO_2}$, $Q1_{Mn_2O_3}$ from the stoichiometry of (1) and the mathematical relationship between $Q2_{Mn_2O_3}$, $Q2_{O_2}$, and Q_{2MnO_2} from the stoichiometry of (2), such that

$$-Q1_{Co(II)EDTA} = -Q1_{MnO_2} = Q1_{Co(III)EDTA} = 2Q1_{Mn_2O_3} \qquad (8)$$

and

$$-Q2_{Mn_2O_3} = -2Q2_{o_2} = \frac{1}{2}Q2_{MnO_2} \qquad (9)$$

The rate of a chemical reaction is usually proportional to the concentrations of reactants raised to some power [Chang, 1984]; therefore, the source/sink terms of (8) and (9) can be written in terms of the reactant species concentrations of (1) and (2):

$$-Q1_{Co(II)EDTA} = -Q1_{MnO_2} = Q1_{Co(III)EDTA} = 2Q1_{Mn_2O_3} = k_{R1}[Co(II)]^{\alpha}[MnO_2]^{\gamma}\left[1-\frac{\Gamma[Mn_2O_3]}{[MnO_2]_{init}}\right] \qquad (10)$$

and

$$-Q2_{Mn_2O_3} = -2Q2_{o_2} = \frac{1}{2}Q2_{MnO_2} = k_{R2}[Mn_2O_3]^{\kappa}[O_2]^{\lambda} \qquad (11)$$

where k_{R1} and k_{R2} are kinetic rate constant, α, γ, κ, and λ are exponential constants that define the reaction order, and $[MnO2]_{init}$ is the initial concentration of β-MnO_2. We have modified (10) to account for a Langmuir-type function that depicts a linear decline in Co(II)EDTA oxidation rates with the increasing α-Mn_2O_3 concentrations. The slope of this linear response is dictated by the constant, Γ. This dimensionless parameter is equivalent to the ratio of the molar mass of β-MnO_2 blocked from reaction to the molar mass of α-Mn_2O_3 precipitated.

Substitution of the relationships given by (10) and (11) into the mass balance equations given by (3) – (7) yields

$$\frac{\partial[Co(II)]}{\partial t} = D\frac{\partial^2[Co(II)]}{\partial x^2} - v\frac{\partial[Co(II)]}{\partial x} - k_{R1}[Co(II)]^{\alpha}[MnO_2]^{\gamma}\left[1-\frac{\Gamma[Mn_2O_3]}{[MnO_2]_{init}}\right] \quad (12)$$

$$\frac{\partial[Co(III)]}{\partial t} = D\frac{\partial^2[Co(III)]}{\partial x^2} - v\frac{\partial[Co(III)]}{\partial x} + k_{R1}[Co(II)]^{\alpha}[MnO_2]^{\gamma}\left[1-\frac{\Gamma[Mn_2O_3]}{[MnO_2]_{init}}\right] \quad (13)$$

$$\frac{\partial[O_2]}{\partial t} = D\frac{\partial^2[O_2]}{\partial x^2} - v\frac{\partial[O_2]}{\partial x} - \frac{k_{R2}}{2}[Mn_2O_3]^{\kappa}[O_2] \quad (14)$$

$$\frac{\rho}{\Theta}\frac{\partial[MnO_2]}{\partial t} = -k_{R1}[Co(II)]^{\alpha}[MnO_2]^{\gamma}\left[1-\frac{\Gamma[Mn_2O_3]}{[MnO_2]_{init}}\right] + 2k_{R2}[Mn_2O_3]^{\kappa}[O_2] \quad (15)$$

$$\frac{\rho}{\Theta}\frac{\partial[Mn_2O_3]}{\partial t} = \frac{k_{R1}}{2}[Co(II)]^{\alpha}[MnO_2]^{\gamma}\left[1-\frac{\Gamma[Mn_2O_3]}{[MnO_2]_{init}}\right] - k_{R2}[Mn_2O_3]^{\kappa}[O_2]^{\lambda} \quad (16)$$

Equations (12) – (16) represent the complete set of equations 'appropriate for describing the transport and fate of reduced and oxidized forms of CoEDTA within the pyrolusite-coated sand columns. These nonlinear equations are solved numerically using a finite-difference method with a predictor-corrector time-stepping scheme for a semi-infinite column with first-type upper boundary conditions for the aqueous species. Zero initial concentrations are assumed for Co(II)EDTA, Co(III)EDTA, and α-Mn_2O_3; the initial O_2 concentration is set at 0.26 mM to reflect equilibrium conditions with the atmosphere, and the initial β-MnO_2 concentration is set at either 0.046 mmol/g for the 0.4%-coated sand or 0.0046 mmol/g for the 0.04%-coated sand.

Parameter Estimation

The parameters that govern the oxidation-reduction reactions and that are required to run the model for CoEDTA transport are k_{R1}, k_{R2}, Γ, a, y, κ, and λ. The exponential constants (i.e., a, y, κ, and λ) can be integers, nonintegers, or even equal to zero [Chang, 1984]. We cannot determine the

values of the exponents *a priori* because these parameters generally are unrelated to the stoichiometry of the reaction [Sposito, 1994]. To reduce the number of fitted parameters, we assume that the values of the exponents are equal to one, and hence, the oxidation-reduction reactions are first-order with respect to each of the reactants.

We identify optimal values of k_{R1}, k_{R2}, and Γ in inverse simulations by using a Levenberg-Marquadt least-squares algorithm to minimize an objective function. The objective function, defined as the sum of the squared residuals between modeled and observed concentrations, is'given by

$$J = \sum_{i=1}^{d} \left[\left([Co(II)]_{\exp_i} - [Co(II)]_i \right) + \left([Co(III)]_{\exp_i} - [Co(III)]_i \right) \right]^2 \qquad (17)$$

where d equals the number of observation times, $[Co(II)]_{\exp_i}$ and $[Co(III)]_{\exp_i}$ are experimental concentrations of Co(II)EDTA and Co(III)EDTA, as measured at the ith observation time and $[Co(II)]_i$ and $[Co(III)]_i$ are modeled concentrations of Co(II)EDTA and Co(III)EDTA, as calculated for the ith observation time.

Results and Discussion

Sensitivity Analysis

Prior to applying the model to the experimental data, we conducted simulations to examine the sensitivity of Co(II)EDTA and Co(III)EDTA breakthrough to changes in k_{R1}, k_{R2}, and I'. Boundary conditions, initial conditions, and flow rate were kept constant across all simulations: influent concentrations of dissolved oxygen, Co(II)EDTA and Co(III)EDTA were 0.26 mM, 0.2 mM, and 0 mM, respectively, solid-phase concentrations of β-MnO_2 and α-Mn_2O_3 at t = 0 were uniform and equal to 0.046 mmol/g and 0 mmol/g, respectively, and the porewater velocity within the 4.5-cm long columns was 27.9 cm/h.

In the first three simulations, we varied k_{R1} over a range of two orders of magnitude, while holding k_{R2} and Γ at zero. When k_{R2} and Γ are both zero, redox dynamics are controlled solely by reaction (1). Oxidation rates increase with the magnitude of k_{R1}, resulting in generation and subsequent breakthrough of progressively higher concentrations of Co(III)EDTA (Figure 4). Nearly all Co(II)EDTA is converted to Co(III)EDTA for k_{R1} equals 1 X 10^3 g $mmol^{-1}h^{-1}$, the highest value tested. Despite this rapid rate of Co(II)EDTA oxidation, the supply of reactive β-MnO_2 is not exhausted as concentrations of Co(III)EDTA remain at elevated levels throughout the course of the simulation (Figure 4).

The next sequence of simulations was aimed at evaluating the response of redox kinetics to solid-phase α-Mn_2O_3 concentrations, assuming that a surface buildup of α-Mn_2O_3 interferes with Co(II)EDTA oxidation. We adjusted values of Γ over an order of magnitude range, while holding k_{R1} at 1 X 10^3 g $mmol^{-1}h^{-1}$ and k_{R2} at zero. For the simulation with Γ = 46, Co(II)EDTA oxidation rates are initially high, but begin to fall slowly after 8 pore volumes (Figure 5). The onset of the decline in Co(II)EDTA oxidation rates occurs sooner and the rapidity of this decline increases as Γ varies from 46 to 460 (Figure 5). These results demonstrate that oxidation kinetics become increasingly sensitive to changes in α-Mn_2O_3 concentrations as Γ increases, or, in other words, for a given α-Mn_2O_3 concentration, the level of Co(II)EDTA oxidation inhibition increases with the magnitude of Γ.

We examined the sensitivity of the model solution to k_{R2}, the rate constant for α-Mn_2O_3 reoxidation, by increasing the magnitude of this parameter from 1 X 10^3 g $mmol^{-1}h^{-1}$ to 1 X 10" g $mmol^{-1}h^{-1}$. For each of these simulations, the values of k_{R1} and Γ were set at 1 X 10^3 g $mmol^{-1}h^{-1}$ and 140, respectively. The dynamics of Co(II)EDTA oxidation for nonzero values of k_{R2} and Γ are affected by the competing processes of β-MnO_2 regeneration, which

enhances Co(II)EDTA oxidation, and occlusion of the β-MnO_2 surface by α-Mn_2O_3, which impedes Co(II)EDTA oxidation. Because the rate of β-MnO_2 restoration increases with the magnitude of k_{R2}, the long-term oxidative potential of the column is greater for higher values of k_{R2} (Figure 6). Consider the simulation for the lowest value of k_{R2} tested. In this case, β-MnO_2 regeneration is slow and relatively low rates of Co(II)EDTA oxidation are maintained under steady-state conditions. For the highest value of k_{R2} tested, on the other hand, α-Mn_2O_3 is reoxidized to β-MnO_2 nearly as rapidly as it forms; thus, complete conversion of Co(II)EDTA to Co(III)EDTA occurs over the entire course of the simulation (Figure 6).

Comparison of Model Calculations and Experimental Data

CoEDTA Transport Through 0.4%-MnO_2-Coated Sand

A qualitative comparison of the measured breakthrough curves to those calculated in the sensitivity analysis indicates that Co(II)EDTA oxidation, as well as β-MnO_2 surface regeneration and Mn_2O_3-induced oxidation inhibition, contribute to the overall fate of CoEDTA in the sand columns. The results of the inverse simulations demonstrate that the model is capable of quantifying the kinetics of these redox processes (Figures 7a, 7b, and 7c). For the three experiments with the 0.4%-coated sand, the model matches the timing and magnitude of the initial peak in Co(III)EDTA concentrations, the rapid decline in Co(III)EDTA concentrations from peak levels, and the eventual stabilization of Co(III)EDTA concentrations at non-zero levels.

The three adjustable parameters, k_{R1}, k_{R2}, and Γ, are estimated well from the breakthrough data; the standard errors of the parameter estimates are less than 15% of the mean values of the parameters (Table 2). The best-fit estimates of the rate constants depend on porewater velocity. As the porewater velocity increases by a factor of four, optimal values of k_{R1} increase from 4.0×10^2 g $mmol^{-1}h^{-1}$ to 3.0×10^3 g $mmol^{-1}h^{-1}$, while optimal values of k_{R2} increase from

7.0×10^3 g $mmol^{-1}h^{-1}$ to 4.0×10^4 g $mmol^{-1}h^{-1}$ (Table 2). The rate constants also vary with changes in influent Co(II)EDTA concentration, but the sensitivity of the rate constants to influent concentration is considerably less than sensitivity of the rate constants to porewater velocity (Table 2). Of the three fitted parameters, Γ shows the least variation with changes in porewater velocity and influent concentration. This parameter is roughly constant across influent concentrations and a four-fold increase in porewater velocity only doubles the optimal value of this parameter (Table 2).

The variation in the model parameters with porewater velocity and influent concentration indicates that the oxidation-reduction reactions probably proceed by several elementary and unobservable steps, not described by the overall reactions from which the rate laws of the model are derived. As such, the kinetics expressions of the model are most properly classified as apparent rate laws. Owing to the great difficult in identifying elementary steps in chemical reactions, the vast majority of studies of reaction kinetics in geologic materials necessarily report apparent, rather than mechanistic rate laws [Skopp, 1986].

We use the optimal values of the apparent rate constants to estimate the time scale for Co(II)EDTA oxidation by β-MnO_2 and the time scale for α-Mn_2O_3 oxidation by dissolved oxygen. These calculations require that both solid-phase β-MnO_2 concentrations and dissolved oxygen concentrations remain constant over the course of the experiment. Results of model simulations of CoEDTA transport through the 0.4%-coated sand show that these conditions are well approximated: the maximum change in β-MnO_2 concentrations along the flow path is less than 3% of the initial β-MnO_2 concentration and oxygen concentrations drop by less than 8% between inlet and outlet boundaries. For constant concentrations of β-MnO_2 and dissolved oxygen, the time scales for Co(II)EDTA oxidation and for α-Mn_2O_3 oxidation are defined on the basis of equations (10) and (11), such that

$$TS_{R1} = \frac{1}{k_{R1}[MnO_2]_{init}} \qquad (18)$$

$$TS_{R2} = \frac{1}{k_{R2}[O_2]_I} \qquad (19)$$

where $[MnO_2]_{init}$ is the initial concentration of β-MnO_2 (0.046 mmol/g) and $[O_2]_I$ is the influent concentration of dissolved oxygen'(0.26 mM). The products in the denominators of (18) and (19) define first-order rate constants for Co(II)EDTA oxidation and for α-Mn_2O_3 oxidation, respectively. The time scales for oxidation can, in turn, be related to the time scale for advective-dispersive transport through a dimensionless Damkohler Number:

$$D_{R1} = \frac{L}{v[TS_{R1}]} \qquad (20)$$

$$D_{R2} = \frac{L}{v[TS_{R2}]} \qquad (21)$$

where L is the is the column length (4.5 cm) and the ratio of L to v gives the time scale for advective transport.

Depending on the experimental treatment, the time scales for Co(II)EDTA oxidation (TS_{R1}) vary from approximately 30 seconds to three minutes, indicating that of Co(II)EDTA is transformed very rapidly to Co(III)EDTA. Because the kinetics of Co(II)EDTA oxidation depend, in part, on α-Mn_2O_3 concentrations, these time-scale calculations apply only to the initial portions of the experiments, when α-Mn_2O_3 exists at very low levels. The Damkohler numbers range from 3 to 5, reflecting that the time scales for transport are comparable to the time scales for reaction. Compared to time scales for advection in the column experiments, times scales for advection in subsurface, environments will be orders of magnitude greater due to lower porewater velocities and longer flow paths; therefore, Co(II)EDTA oxidation in natural systems will be characterized by

large values of D_{R1} and the redox reaction will proceed at rates that are essentially instantaneous, relative to the rate of groundwater flow. The time scales for α-Mn_2O_3 oxidation (TS_{R2}) are on the order of hours, and the corresponding Damkohler Numbers vary from 0.08 to 0.12; therefore, regeneration of β-MnO_2 through oxidative transformation of the surface-bound precipitate occurs much more slowly than the rates of Co(II)EDTA oxidation.

The rate of the CoEDTA redox reaction declines with time, presumably due to the formation of α-Mn_2O_3 over the reactive β-MnO_2 surface. We simulate the decline in oxidation rates with a linear relationship governed by Γ, a constant that quantifies the molar mass of β-MnO_2 blocked by the precipitation of α-Mn_2O_3. Calculations based on the best-fit values of Γ demonstrate that small accumulations of α-Mn_2O_3 are capable of occluding large amounts of β-MnO_2 (Figure 8). The precipitous decline in the reactive fraction of β-MnO_2 with increasing α-Mn_2O_3 levels suggests that β-MnO_2 must occur on the sand as a multi-layered deposit, and that during the initial stages of the experiments, reductive transformation of the outermost layers generates a thin skin of α-Mn_2O_3 that effectively shields the bulk of the β-MnO_2 from reaction with Co(II)EDTA. Because α-Mn_2O_3 is an insoluble precipitate it cannot be swept from the surface with the advecting pore fluid, and hence, the β-MnO_2 associated with the layers that underlie the α-Mn_2O_3 rind is never exposed during the course of the experiments.

CoEDTA Transport Through 0.04%-MnO_2-Coated Sand

Three separate experiments were conducted in the same column of 0.04%-coated sand. In between each experiment, the column was flushed with CoEDTA-free water for a period of 12 – 23 pore volumes in an effort to restore the oxidative potential of the column [Jar-dine and Taylor, 1995b]. In order to simulate the periods of column flushing, together with the periods of Co(II)EDTA injection, we modified the model to account for a time-dependent boundary condition.

That is, the influent boundary concentration of Co(II)EDTA was set to 0.2 mM to simulate a period of Co(II)EDTA injection and to 0 mM to simulate a period of column flushing with Co(II)EDTA-free water. Both the CoEDTA-containing water and the Co(II)EDTA-free water were fully oxygenated, so the concentration of dissolved oxygen at the influent boundary was held steady at 0.26 mM for the duration of the simulation.

The simulation of CoEDTA transport through the 0.04%-coated sand represents a very rigorous test of the model because the model is required to account for the variation associated with three different sets of breakthrough curves with a single set of optimal parameters. In light of the rigor of the test, agreement between model calculations and experimental data is quite good (Figure 9). For each of the three breakthrough curves, the model underestimates Co(III)EDTA concentrations (and hence, overestimates Co(II)EDTA concentrations) at steady state; however, the magnitude of these model-data discrepancies is small. The model matches the key feature of the second and third breakthrough curves, the rapid increase in Co(III)EDTA concentrations that follows column flushing and that indicates a temporary restoration of the oxidative capacity of the column. Thus, we infer that we have accurately quantified the kinetics of the reaction responsible for generating β-MnO_2 from α-Mn_2O_3.

The model also reproduces the onset and the rate of the decline in Co(III)EDTA concentrations, which provides additional evidence that we have identified a suitable form of the mathematical function for Mn_2O_3-induced inactivation of the β-MnO_2 surface. The optimal value of Γ is greater for this simulation than for the simulations of CoEDTA transport in the 0.4%-coated sand, signifying that the mass of β-MnO_2 occluded per mass of α-Mn_2O_3 precipitated is greater in the experiments with the 0.4%-coated sand, relative to the experiments with the 0.04%-coated sand (Table 2). We attribute differences in the α-Mn_2O_3 blocking efficiency to differences in way that

β-MnO_2 is distributed on the 0.04% and 0.4%-coated sand. Jardine and Taylor [1995b] analyzed the sands with scanning electron microscopy and high resolution transmission electron microscopy, and reported that 0.4%-coated material consisted of aggregates of β-MnO_2, while the 0.04% material was not aggregated, but spread uniformly across the surfaces of the quartz grains. Because β-MnO_2 is aggregated at heavier surface coverages, a small mass of α-Mn_2O_3 that forms around the exterior of the aggregates covers a disproportionately large mass of the β-MnO_2. In comparison, the even distribution of β-MnO_2 on the 0.04%-coated media effectively reduces the mass of β-MnO_2 that a given mass of α-Mn_2O_3 can occlude.

Summary and Conclusions

We have confirmed that two nonlinear reactions control CoEDTA transformation, and we have identified the appropriate structure of a mathematical model for quantifying the kinetics of these reactions. On a fresh surface of β-MnO_2, the rate of Co(II)EDTA transformation to Co(III)EDTA is rapid, with time-scales for oxidation on the order of minutes. Thus, even in subsurface environments dominated by preferential flow processes, where porewater and dissolved solutes have short residence times, the extent of oxidative transformation of Co(II)EDTA can be substantial. Although initial oxidation rates are fast, Co(II)EDTA oxidation rates diminish as contact times increase due to formation of α-Mn_2O_3, an insoluble reaction product that limits the exposure of the reactive β-MnO_2 surface. We quantified the dependence of Co(II)EDTA oxidation rates on α-Mn_2O_3 concentrations in terms of a Langmuir-type blocking function, which describes a linear decline in Co(II)EDTA reaction rates with increasing α-Mn_2O_3 concentrations. This approach has applicability outside the experimental system investigated here as time-dependent decreases in the reactivity of manganese minerals toward the oxidation of other contaminants, such

as chromium, have been widely observed and have been linked to reaction products that poison the redox-reactive surface [e.g., Amacher and Baker, 1982; Eary and Rai, 1987; Fendorf et al., 1993].

Accumulation of α-Mn_2O_3 slows the rates of Co(II)EDTA conversion to Co(III)EDTA; however, the oxidative potential of the sand beds is not totally depleted, even after extended periods of reaction. Our work offers further evidence that regeneration of fresh β-MnO_2 surface through reoxidation of α-Mn_2O_3 by dissolved oxygen sustains low levels of Co(II)EDTA oxidation. Thus, the long-term production of Co(III)EDTA, the more mobile and more stable of the two cobalt species, ultimately depends on the rate of conversion of α-Mn_2O_3 to β-MnO_2, which, in turn, depends on the availability of porewater oxygen.

The kinetics of α-Mn_2O_3 oxidation by dissolved oxygen has not been quantified prior to our work. As dissolved oxygen is consumed during α-Mn_2O_3 oxidation, the most direct way to test the proposed reaction scheme (given by (2)) is by comparing modeled and measured concentrations of dissolved oxygen. Because these data are unavailable, we evaluated the reaction scheme for α-Mn_2O_3 oxidation by testing the model to simulate simultaneously concentrations of Co(II)EDTA and Co(III)EDTA, both of which depend on the kinetics of α-Mn_2O_3 oxidation. We find that experimental data on Co(II)EDTA and Co(III)EDTA concentrations are well described by assuming that rate of α-Mn_2O_3 oxidation is directly proportional to the concentrations of α-Mn_2O_3 and dissolved oxygen. Although lower than initial rates of Co(II)EDTA oxidation, model results show that the kinetics of α-Mn_2O_3 oxidation are reasonably rapid, with reaction time-scales in the range of hours.

Our results demonstrate that, even in a Iaboratory system characterized by simple aqueous chemistry and by only one redox-reactive solid phase, a complex suite of processes governs the dynamics of CoEDTA oxidation-reduction. The work reported here documents a tested theoretical

approach for quantifying interactions between hydrological and geochemical processes in a model experimental system, and forms a basis from which to study coupled mass transport and oxidation-reduction in natural systems of greater physical and chemical complexity. Continued advances in our current understanding of the subsurface migration of redox-sensitive contaminants ultimately will rely on research that integrates laboratory and field experimentation with mathematical modeling.

References

Amacher, M.C. and D.A. Baker, Redox reactions involving chromium, plutonium, and manganese soils, final report DE-AS08-77DP04515; Institute for Research on Land and Water Resources, Penn. State University, **1982.**

Brooks, S.C., D.L. Taylor, and P.M. Jardine, Reactive transport of EDTA-complexed cobalt in the presence of ferrihydrite, *Geochim. Cosmochim. Acta*, *60,* 1899-1908, 1996.

Bums, R.G., The uptake of cobalt into ferromanganese nodules, soils, and synthetic Mn(IV) oxides, *Geochim. Cosmochim. Acta*, 40, 95-102, 1976.

Chang, R., Chemistry, 824 pp., Random House, Inc., New York, 1984.

Eary, L.E. and Rai, D., Kinetics of chromium(III) oxidation by chromium(VI) reaction with manganese dioxide, *Environ. Sci. Technol.*, 21, 1187-l 193, 1987.

Fendorf, S.E., R.J. Zasoski, and R. G. Burau, Competing metal ion influences on chromium(III) oxidation by bimessite, *Soil* Sci. *Soc. Am. J.,* 57, 1508-1515, 1993.

Fendorf, S., P.M. Jardine, R.R. Patterson, D.L. Taylor, and S.C. Brooks, Pyrolusite surface transformations measured in real-time during the reactive transport of Co(II)EDTA, *Geochim. Cosmochim. Acta*, 63, 3049-3057, 1999.

Friedly, J.C., J.A. Davis, and D.B. Kent, Modeling hexavalent chromium reduction in groundwater in field-scale transport and laboratory batch experiments, *Water Resour. Res., 3 1, 2783-*2794, 1995.

Girvin, D.C., P.L. Gassman, and H. Bolton, Jr., Adsorption of aqueous cobalt ethylenediaminetetraacetate by Al_2O_3, Soil *Sci. Soc. Am. J.,* 57, 47-57, *1993.*

Jardine, P.M., G.K. Jacobs, and J.D. O'Dell, Unsaturated transport processes in undisturbed heterogeneous porous media, II. Co-contaminants, *Soil Sci. Soc. Am. J., 57, 954-962,* 1993.

Jardine, P.M. and D.L. Taylor, Fate and transport of ethylenediaminetetraacetate chleated contaminants in subsurface environments, *Geoderma*, *67*, 125-140, 1995a.

Jardine, P.M. and D.L. Taylor, Kinetics and mechanisms of Co(II)EDTA oxidation by pyrolusite, *Geochim. Cosmochim. Acta*, 59, 4193-4203, 1995b.

Killey, R.W.D., J.O. McHugh, D.R. Champ, E.L. Cooper,-and J.L. Young, Subsurface cobalt-60 migration from a low-level waste disposal site, *Environ, Sci. Technol.*, 18, 148-157, 1984.

Liu, C.W. and T.N. Narasimhan, Redox-controlled multiple-species reactive chemical transport, 1. Model development, *Water Resour. Res.*, 25, 869-882, 1989.

Means, J.L., D.A. Crerar, M.P. Borscik, and J.O. Duguid, Migration of radioactive wastes: radionuclide mobilization by complexing agents, *Science, 200,* 1477-148 1, 1978.

Murray, J.W. and J.G. Dillard, The oxidation of cobalt(II) adsorbed on manganese dioxide, *Geochim. Cosmochim. Acta*, 43, 781-787, 1979.

Parker, D.R., L.W. Zelazny, and T.B. Kinraide, Improvements to the program GEOCHEM, *Soil Sci. Soc. Am. J.*, 51, 488-491, 1987.

Skopp, J., Analysis of time-dependent chemical processes in soils, *J. Environ. Qual.*, 15:205-213, 1986.

Sposito, G. and S.V. Mattigod, *GEOCHEM: Computer Program for the Calculation of Chemical Equilibria in Soil Solutions and Other Natural Water Systems,* Keamey Found. of Soil Sci. Univ. California, Riverside, CA, 1980.

Sposito, *G., Chemical Equilibria and Kinetics in Soils, 268* pp., Oxford University Press, New York, 1994.

Szecsody, J.E., J.M. Zachara, and P.L. Bruckhart, Adsorption-dissolution reactions affecting the distribution and stability of Co(II)EDTA in iron oxide-coated sand, *Environ. Sci. Technol.*, 28, 1706-1716, 1994.

Szecsody, J.E., J.M. Zachara, A. Chilakapati, P.M. Jardine, and A.S. Ferrency, Importance of flow and particle-scale heterogeneity on $Co^{II/III}$EDTA reactive transport, *J. Hydrol.*, *209,* 112-136, 1998a.

Szecsody, J.E., A. Chilakapati, J.M. Zachara, and A. Garvin, Influence of iron-oxide inclusion shape on $Co^{II/III}$EDTA reactive transport through spatially heterogeneous sediment, *Water Resour. Res.,* 34, 2501, 2514, 1998b.

Xue Y. and S.J. Traina, Oxidation kinetics of Co(II)EDTA in aqueous and semi-aqueous goethite suspensions, *Environ, Sci. Technol.*, *30,* 1975-1981, 1996.

Yeh, G.T. and K. Salvage, HYDROGEOCHEM 2.1: A coupled model of hydrologic transport and geochemistry with both equilibrium and kinetic reactions, *Penn State University Dept of Civil and Environ. Eng. Tech. Rep., 1995.*

Zachara, J.M., S.C. Smith, and L.S. Kuzel, Adsorption and dissociation of Co-EDTA complexes in iron oxide containing subsurface sands, *Geochim. Cosmochim. Acta*, 59, 4825-4839, 1995a.

Zachara, J.M., P.L. Gassman, S.C. Smith, and D. Taylor, Oxidation and adsorption of Co(II)$EDTA^{2-}$ complexes in subsurface materials with iron and manganese oxide grain coatings, *Geochim. Cosmochim. Acta*, 59, 4449-4463, 1995b.

Figure Legends

Figure 1. Experimental breakthrough curves for the displacement of a 0.2 mM Co(II)EDTA solution through a packed bed of 0.4% pyrolusite-coated sand at an average linear pore water velocity of 27.9 cm/h. Co(II)EDTA was applied to the top of the column continuously throughout the course of the experiment. An expanded view of the initial 20 pore volumes of the CoEDTA breakthrough is shown in Figure 2a. The bromide breakthrough curve was measured in the same media and at the same fl ow rate.

Figure 2. Experimental breakthrough curves for the displacement of Co(II)EDTA solution through 0.4% pyrolusite-coated sand. The three experiments are distinguished on the basis of influent Co(II)EDTA concentration, $Co(II)_o$, and average linear pore water velocity, v. The asterisks represent measured concentrations of Co(II)EDTA; the open circles represent measured concentrations of Co(III)EDTA. Only the first 20 pore volumes of breakthrough are shown in order to best illustrate the differences between experimental treatments.

Figure 3. Breakthrough curves measured for experiments on the sequential displacement of 0.2 mM Co(II)EDTA through 0.04% β-MnO_2-coated sand: (a) initial displacement experiment, (b) repeated displacement experiment on the same column following a 12-pore volume flush with oxygenated water, and (c) repeated Co(II)EDTA displacement experiment on the same column following a 23-pore volume flush with oxygenated water. The concentrations of Co(II)EDTA (asterisks) and Co(III)EDTA (open circles) are plotted in terms the cumulative number of pore volumes of water eluted through the columns.

Figure 4. Sensitivity of calculated concentrations of Co(II)EDTA (solid lines) and Co(III)EDTA (dashed lines) to variation in k_{R1}. Values used for k_{R1}: (a) 10 g $mmol^{-1}h^{-1}$, (b) 100 g $mmol^{-1}h^{-1}$, and (c) 1 X 10^3 g $mmol^{-1}h^{-1}$. Both k_{R2} and Γ were assigned values of zero for the three simulations.

Figure 5. Sensitivity of calculated concentrations of Co(II)EDTA (solid lines) and Co(III)EDTA (dashed lines) to variation in Γ. Values used for Γ: (a) 46, (b) 140, and (c) 460. The modeled results were obtained for $k_{R1} = 1 \times 10^3$ g mmol^{-1}h^{-1} and $k_{R2} = 0$.

Figure 6. Sensitivity of calculated concentrations of Co(II)EDTA (solid lines) and Co(III)EDTA (dashed lines) to variation in k_{R2}. Values used for k_{R2}: (a) 1×10^3 g mmol^{-1}h^{-1}, (b) 5×10^3 g mmol^{-1}h^{-1}, and (c) 1×10^4 g mmol^{-1}h^{-1}. The modeled results were obtained for $k_{R1} = 1 \times 10^3$ g mmol^{-1}h^{-1} and $\Gamma = 140$.

Figure 7. Experimental breakthrough curves (open circles and asterisks) and model-calculated breakthrough curves (solid lines and dashed lines) for the displacement of Co(II)EDTA solution through 0.4% pyrolusite-coated sand. The three experiments are distinguished on the basis of infl uent Co(II)EDTA concentration, $Co(II)_o$, and average linear pore water velocity, v.

Figure 8. The relationship between the surface concentration of α-Mn_2O_3 precipitate and the fraction of β-MnO_2 that is available to oxidize Co(II)EDTA. The fraction of β-MnO_2 available for reaction is defined in terms of a Langmuir-type blocking function and is equal to $1 - \Gamma[Mn_2O_3]/[MnO_2]_{init}$. Best-fit values of Γ used to calculate the Langmuir-type relationship are given in Table 2.

Figure 9. Experimental breakthrough curves (open circles and asterisks) and model-calculated breakthrough curves (solid lines and dashed lines) for the sequential displacement of 0.2 mM Co(II)EDTA through 0.04% β-MnO_2-coated sand: (a) initial displacement experiment, (b) repeated displacement experiment on the same column following a 12-pore volume flush with oxygenated water, and (c) repeated Co(II)EDTA displacement experiment on the same column following a 23-pore volume flush with oxygenated water. Solutions to the model equations were fit

simultaneously to the three sets of breakthrough curves, producing a single set of optimal parameters (see Table 2).

Table 1. Measurements of average linear porewater velocity (v), influent Co(II)EDTA concentration ($Co(II)_o$), initial solid-phase pyrolusite concentration ($[MnO_2]_{init}$), and the length of time that a solution with a Co(II)EDTA concentration of $Co(II)_o$ is applied to the columns (TP).

Experiment Number[χ]	v (cm/h)	$Co(II)_o$ (mM)	$[MnO_2]_{init}$ (g MnO_2/g sand)	TP (pore volumes)
1	27.9	0.2	4.0×10^{-2}	68.0
2	27.9	0.8	4.6×10^{-2}	13.6
3	110.8	-0.2	4.6×10^{-2}	35.7
4	27.9	0.2	4.6×10^{-3}	44.3
4b[#]	27.9	0.0	4.6×10^{-3}	12.4
5	27.9	0.2	4.6×10^{-3}	7.6
5b[#]	27.9	0.0	4.6×10^{-3}	22.9
6	27.9	0.2	4.6×10^{-3}	6.2

[χ]Experiments l-3 were each conducted with freshly packed columns; experiments 4-6 were conducted on the same column.

#Columns were flushed with CoEDTA-free water in experiments 4b and 5b, and hence, $Co(II)_o$ equals zero.

Table 2. Fitted parameters (with standard errors).

Experimental Treatment				Best-Fit Parameter Values.		
Number	v (cm/h)	C_o (mM)	$[MnO_2]_{init}$ (mm01 /g)	k_{R1} X 10^2 (g mmol-'h-l)	k_{R2} X 10^3 (g mmol-'h-l)	Γ
1	27.9	0.2	4.6 X10^{-2}	3.95 (0.27)	7.01 (0.83)	203.46 (2.18)
2	27.9	0.8	4.6 X10^{-2}	5.57 (0.50)	16.7 (1.61).	166.52 (0.94)
3	110.8	0.2	4.6 X10^{-2}	29.66 (4.29)	39.67 (4.0)	454.48 (2.86)
4-6	27.9	0.2/0.0	4.6 X10^{-3}	72.71 (5.11)	2.58 (0.15)	68.36 (2.16)

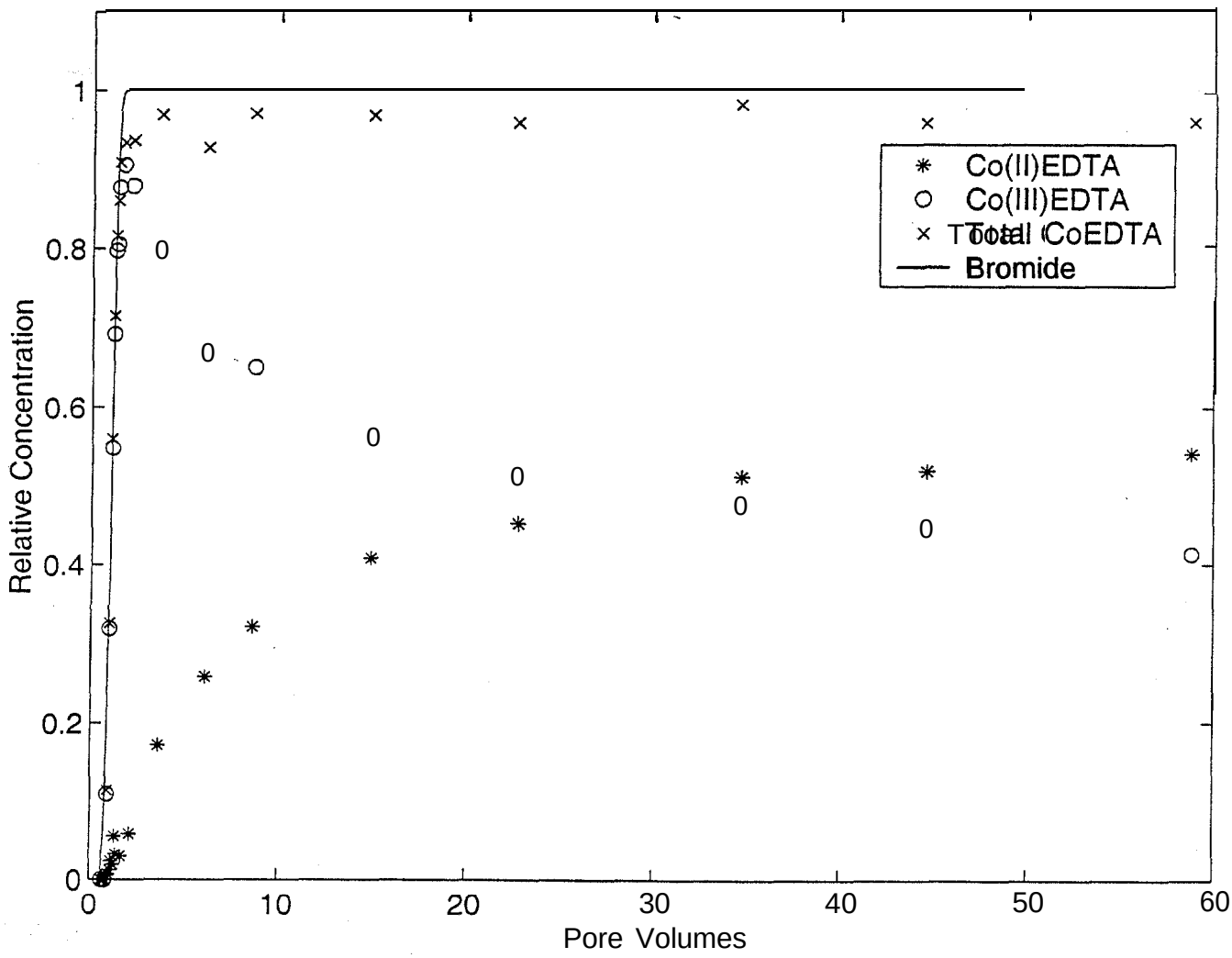
Relative Concentration
Pore Volumes
0
0.2
0.4
0.6
0.8
1
0
10
20
30
40
50
60
Co(II)EDTA
Co(III)EDTA
Total CoEDTA
Bromide

Figure 1.

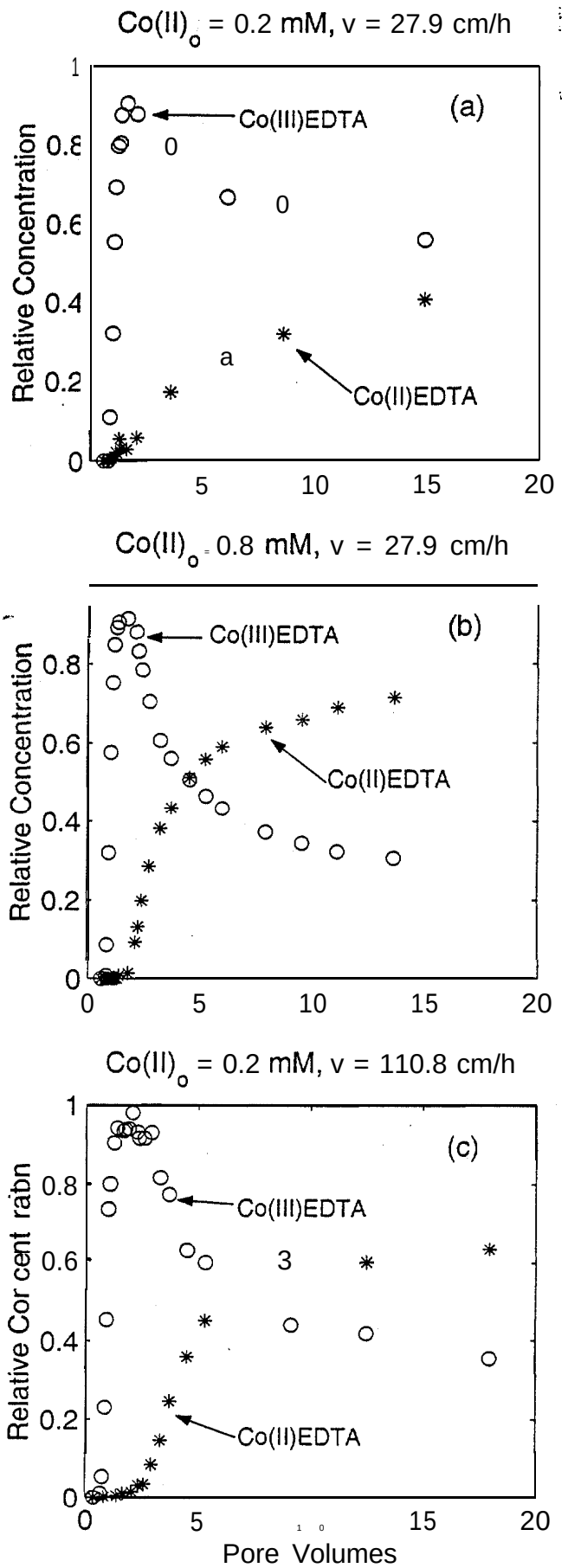
Co(II)o = 0.2 mM, v = 27.9 cm/h
(a)
Co(III)EDTA
Co(II)EDTA
Relative Concentration
Co(II)o = 0.8 mM, v = 27.9 cm/h
(b)
Co(III)EDTA
Co(II)EDTA
Relative Concentration
Co(II)o = 0.2 mM, v = 110.8 cm/h
(c)
Co(III)EDTA
Co(II)EDTA
Relative Concentration
Pore Volumes

Figure 2.

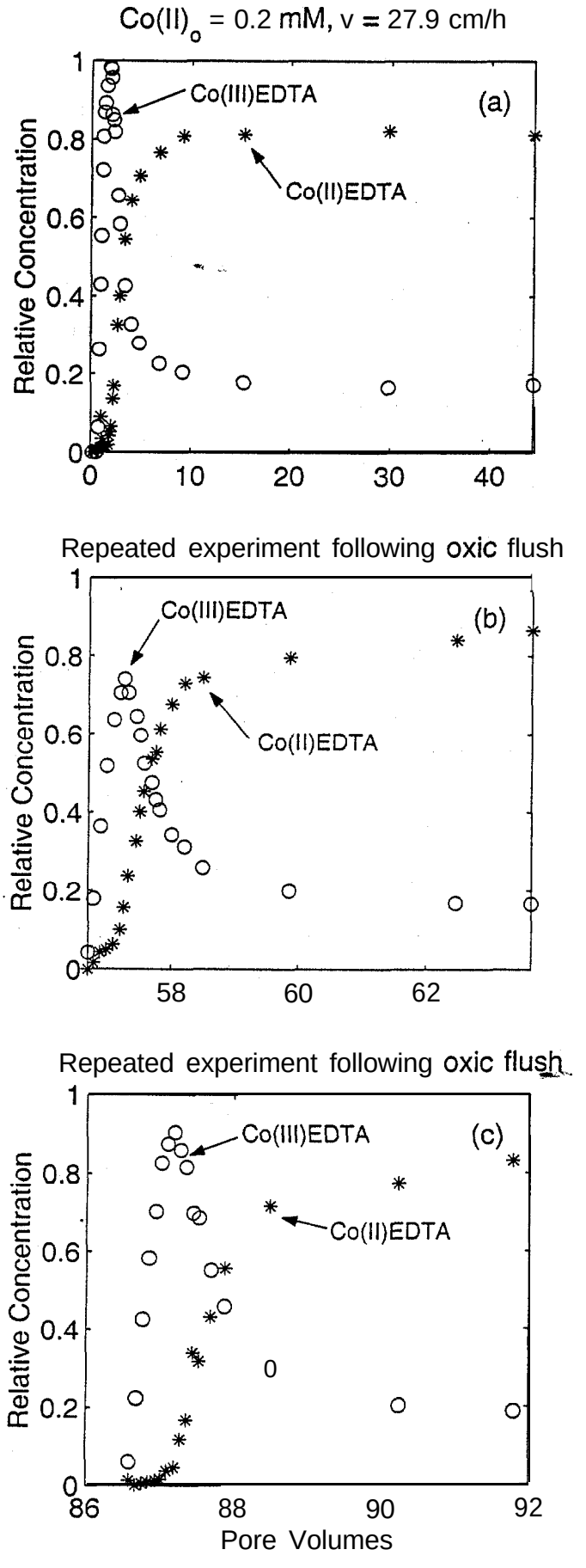
Co(II)$_o$ = 0.2 mM, v = 27.9 cm/h
Co(III)EDTA
Co(II)EDTA
(a)
Relative Concentration
Repeated experiment following oxic flush
Co(III)EDTA
Co(II)EDTA
(b)
Relative Concentration
Repeated experiment following oxic flush
Co(III)EDTA
Co(II)EDTA
(c)
Relative Concentration
Pore Volumes

Figure 3.

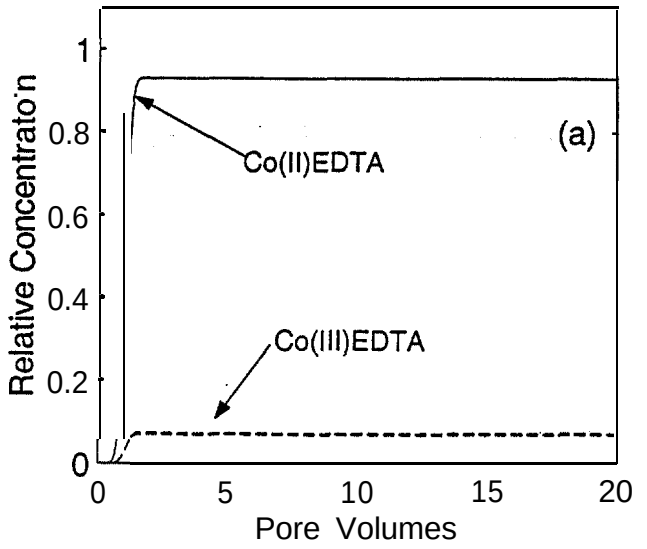
Relative Concentrato'n
1
0.8
0.6
0.4
0.2
0
0
5
10
15
20
Pore Volumes
(a)
Co(II)EDTA
Co(III)EDTA

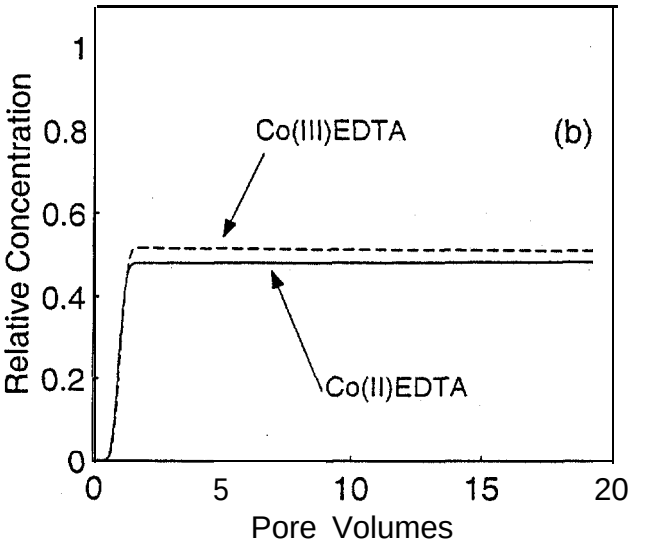
Relative Concentration
1
0.8
0.6
0.4
0.2
0
0
5
10
15
20
Pore Volumes
(b)
Co(III)EDTA
Co(II)EDTA

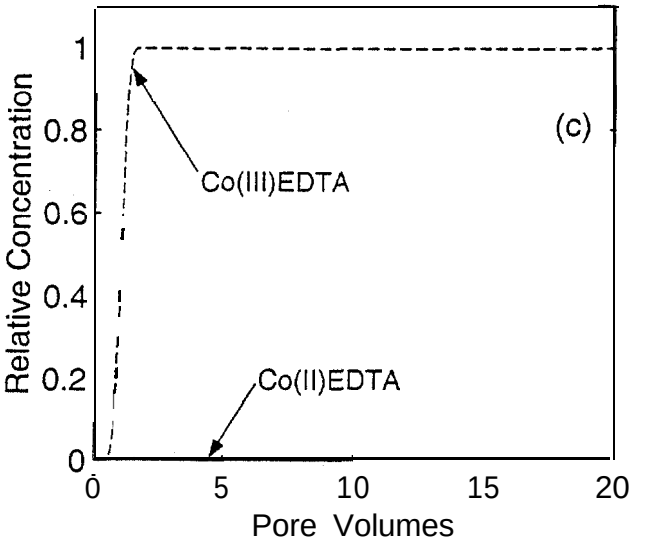
Relative Concentration
1
0.8
0.6
0.4
0.2
0
0
5
10
15
20
Pore Volumes
(c)
Co(III)EDTA
Co(II)EDTA

Figure 4.

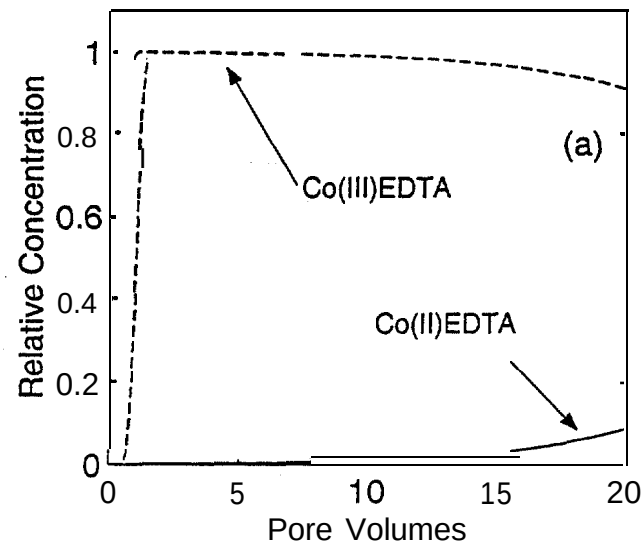
Relative Concentration
1
0.8
0.6
0.4
0.2
0
0
5
10
15
20
Pore Volumes
(a)
Co(III)EDTA
Co(II)EDTA

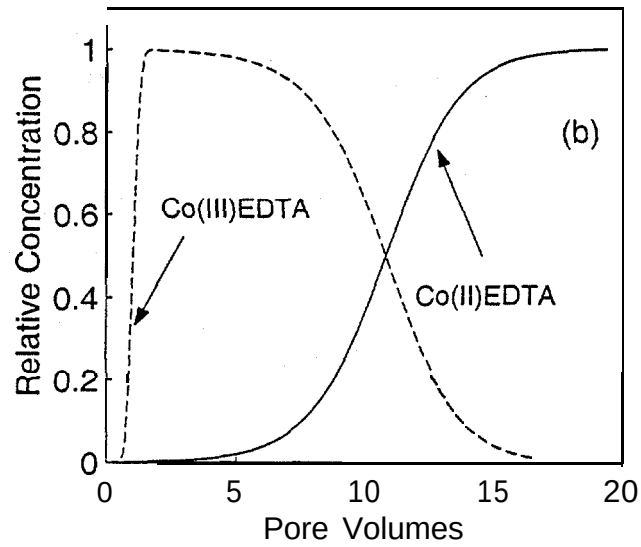
Relative Concentration
1
0.8
0.6
0.4
0.2
0
0
5
10
15
20
Pore Volumes
(b)
Co(III)EDTA
Co(II)EDTA

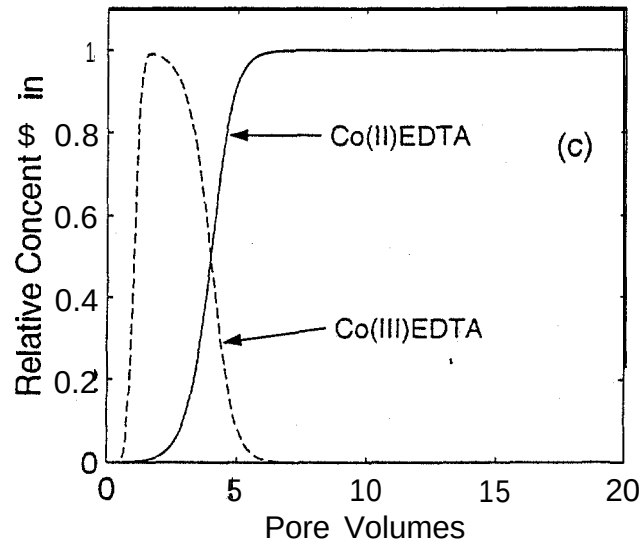
Relative Concent $ in
1
0.8
0.6
0.4
0.2
0
0
5
10
15
20
Pore Volumes
(c)
Co(II)EDTA
Co(III)EDTA

Figure 5.

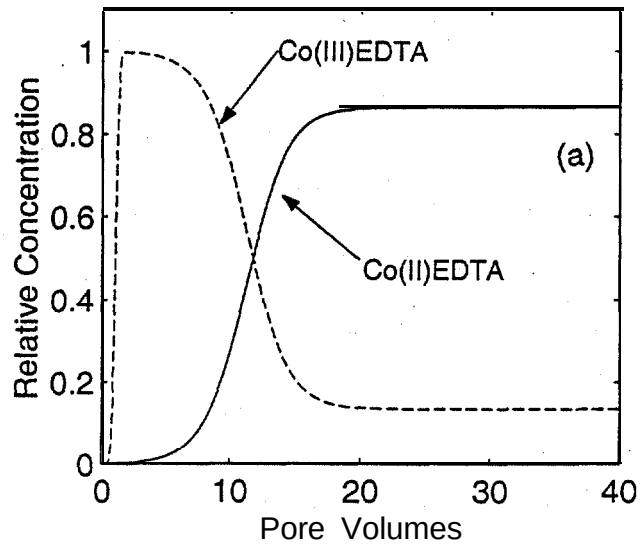
Co(III)EDTA
Co(II)EDTA
(a)
Relative Concentration
Pore Volumes
0
0.2
0.4
0.6
0.8
1
0
10
20
30
40

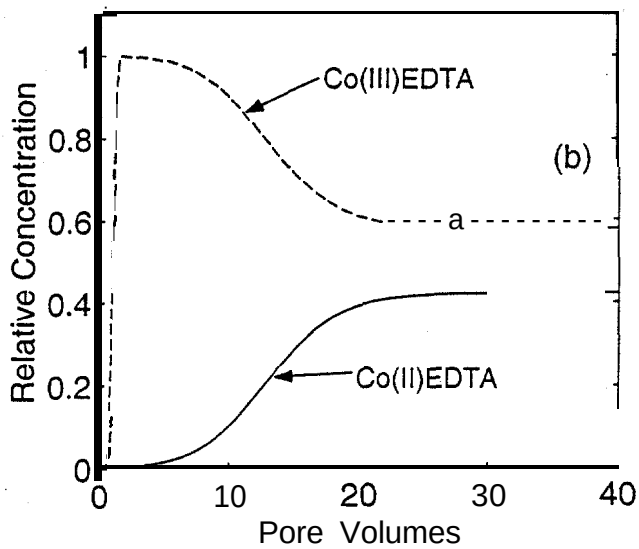
Co(III)EDTA
Co(II)EDTA
(b)
a
Relative Concentration
Pore Volumes
0
0.2
0.4
0.6
0.8
1
0
10
20
30
40

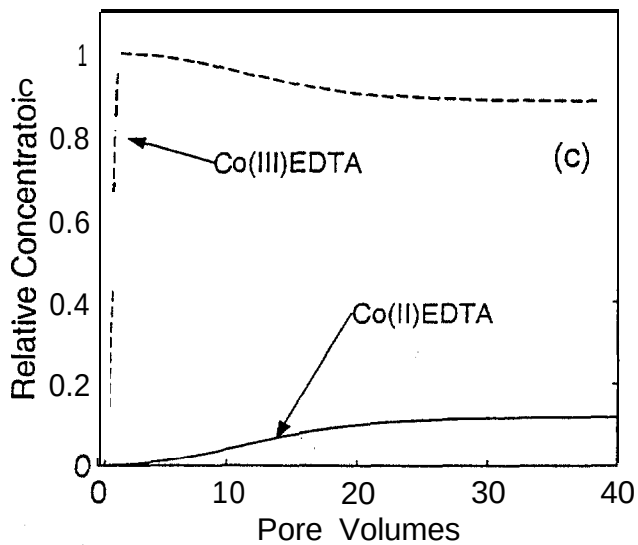
Co(III)EDTA
Co(II)EDTA
(c)
Relative Concentratoic
Pore Volumes
0
0.2
0.4
0.6
0.8
1
0
10
20
30
40

Figure 6.

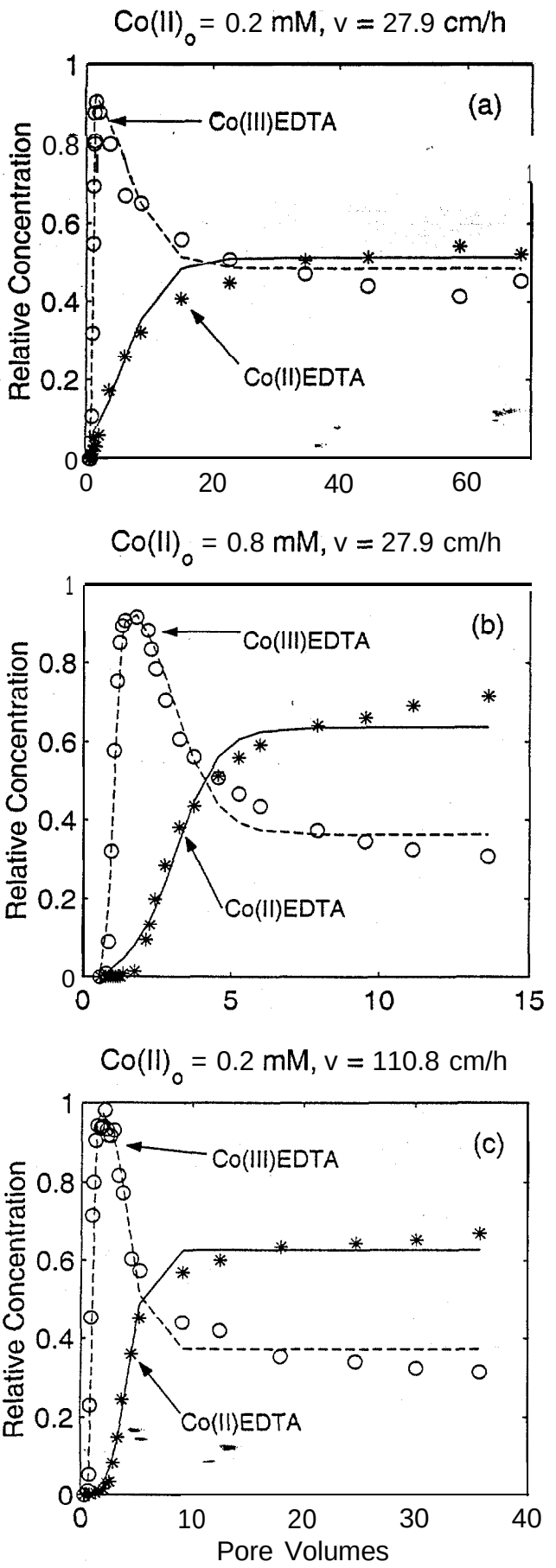
Co(II)$_o$ = 0.2 mM, v = 27.9 cm/h
(a)
Co(III)EDTA
Co(II)EDTA
Relative Concentration
Co(II)$_o$ = 0.8 mM, v = 27.9 cm/h
(b)
Co(III)EDTA
Co(II)EDTA
Relative Concentration
Co(II)$_o$ = 0.2 mM, v = 110.8 cm/h
(c)
Co(III)EDTA
Co(II)EDTA
Relative Concentration
Pore Volumes

Figure 7.

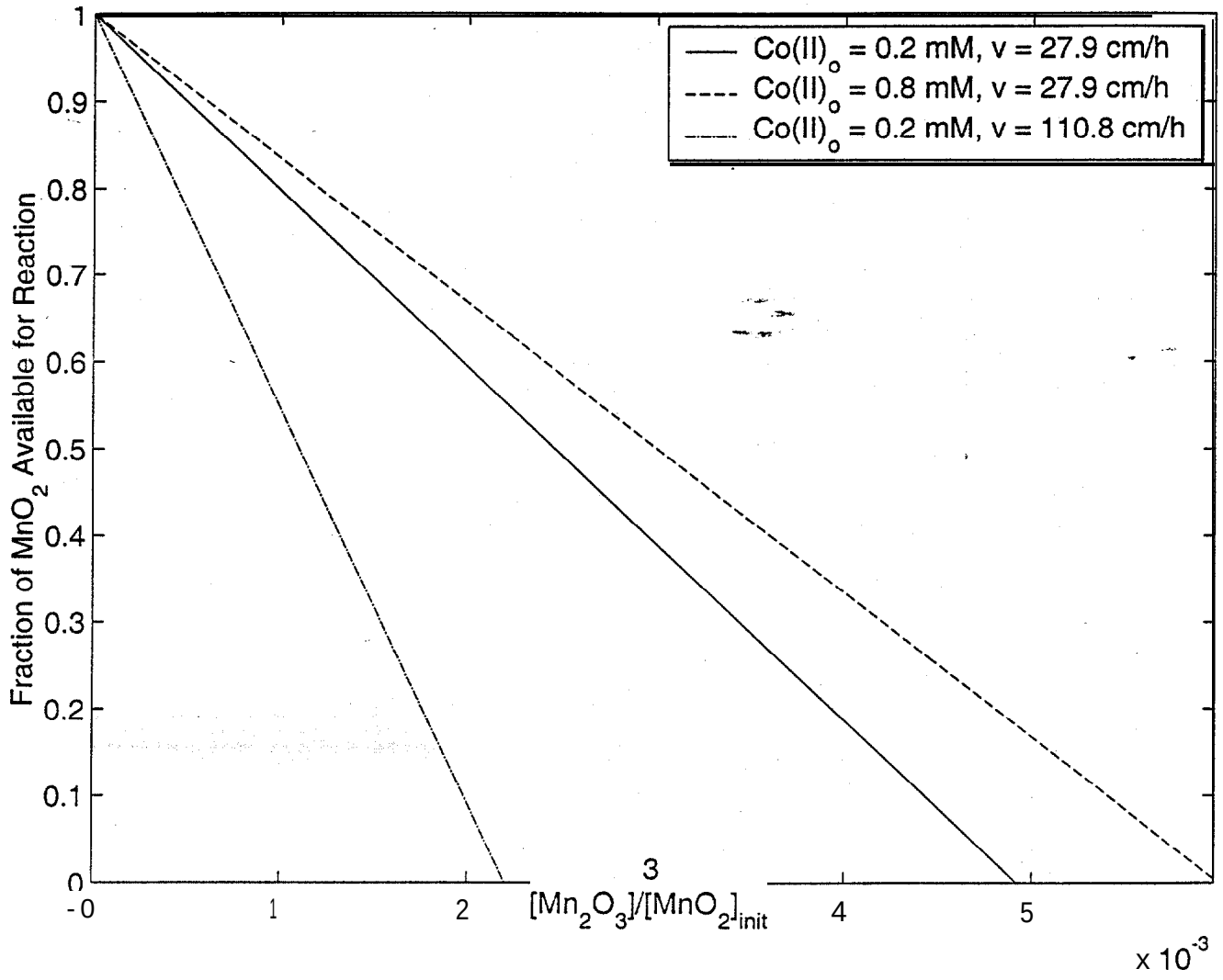
Co(II)$_o$ = 0.2 mM, v = 27.9 cm/h
Co(II)$_o$ = 0.8 mM, v = 27.9 cm/h
Co(II)$_o$ = 0.2 mM, v = 110.8 cm/h
Fraction of MnO_2 Available for Reaction
$[Mn_2O_3]/[MnO_2]_{init}$
x 10^{-3}
1
0.9
0.8
0.7
0.6
0.5
0.4
0.3
0.2
0.1
0
-0
1
2
3
4
5

Figure 8.

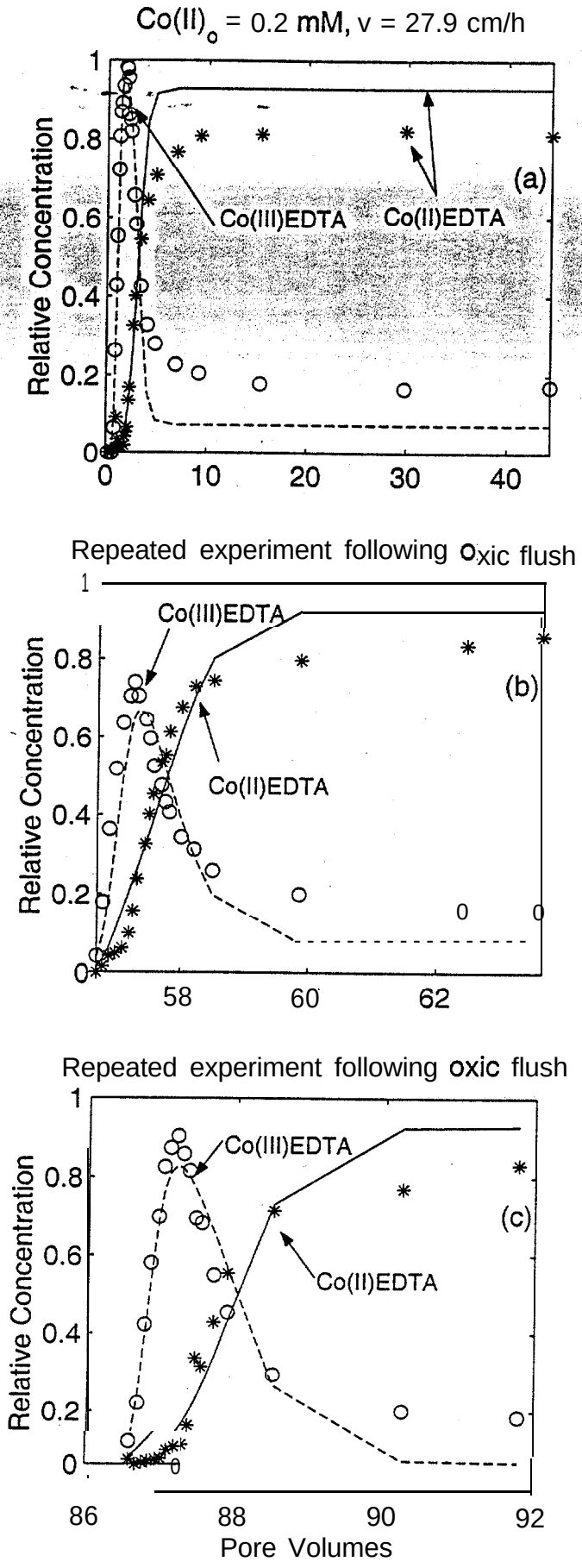
Co(II)$_o$ = 0.2 mM, v = 27.9 cm/h
Relative Concentration
Co(III)EDTA
Co(II)EDTA
(a)
Repeated experiment following oxic flush
Co(III)EDTA
Co(II)EDTA
(b)
Repeated experiment following oxic flush
Co(III)EDTA
Co(II)EDTA
(c)
Pore Volumes

Figure 9.